Ibn Al-Haitham Journal for Pure and Applied Sciences
Journal homepage: jih.uobaghdad.edu.iq
PISSN: 1609-4042, EISSN: 2521-3407
IHJPAS. 2025, 38(3)

Preparation and Characterization of $rGO/Fe_3O_4/MnO_2$ Nanocomposite for Enhanced Removal of Terasil Black Dye in Waste Water Treatment

Ali Fadhil Ismail [1*] and Entisar E. Al-Abodi [2]
[1,2] Department of Chemistry, College of Education for Pure Science (Ibn Al-Haitham), University of Baghdad, Baghdad, Iraq.
*Corresponding Author.

Received: 10 December 2024 Accepted: 23 April 2024 Published: 20 July 2025
doi.org/10.30526/38.3.4069

Abstract

This study focuses on the synthesis and characterization of a ternary nanocomposite comprising reduced graphene oxide (rGO), magnetite (Fe_3O_4), and manganese dioxide (MnO_2) nanoparticles (NPs). The aim of using it is to remove Terasil Black dye from water, particularly in textile industries. The nanocomposite was created using a co-precipitation method, followed by physical bonding with MnO_2 NPs. The structural properties, surface morphology, and elemental composition were evaluated through X-ray diffraction (XRD), Field Emission Scanning Electron Microscopy (FESEM), and energy-dispersive X-ray (EDX) analysis. The XRD results confirmed the presence of an amorphous phase along with distinct diffraction peaks that correspond to specific lattice planes. FESEM images showed irregular particle shapes and significant agglomeration. EDX analysis confirmed the presence of the expected elements. The adsorption isotherms displayed (S) patterns as classified by Giles, suggesting that the dye ions align vertically relative to the nanocomposite's surface. The adsorption process is endothermic and primarily driven by physical interactions, which become more significant at higher temperatures. Analyzing the adsorption data indicates that the Freundlich isotherm model better describes this process, suggesting a non-uniform surface. This model demonstrates that chemical and physical adsorption processes were involved, with their contributions varying across different temperature ranges. The findings provide valuable insights into the thermodynamics and kinetics of dye adsorption on $rGO/Fe_3O_4/MnO_2$ nanocomposites, which are essential for optimizing their application in waste water treatment.

Keywords: Adsorption, Manganese oxide nanoparticles, Reduced graphene oxide, Terasil black dye, Waste water.

1. Introduction

The adsorbents of waste water obtained through the nanomaterials carbon graphene were applied in the water treatment to solve the water clean-up problem (1). Applying the Hummer method, which involves the preparation of graphene oxide moiety and then inserting the metal nanoparticles (NPs), achieves the desired product (2). Such a novel method, through adsorption phenomena, identifies the centers of the material that increase their number

© 2025The Author(s). Published by College of Education for Pure Science (Ibn Al-Haitham), University of Baghdad. This is an open-access article distributed under the terms of the Creative Commons Attribution 4.0 International License

compared to the conventional adsorbents. The centers of the material approach the contaminants, such as lead or dyes, from water, owing to the advantage of this phenomenon (3). Graphene, considered the thinnest form of the carbon family, is heated weirdly. Furthermore, graphene has unique chemical, mechanical, and electrical properties that it will use to absorb electromagnetic waves faster and thus increase efficiency (4,5).This property makes the graphene array matrices highly viable for many fields and applications involving, among others, strong structures, the environment, energy production, storage, and renewal, because of its exceptional electrical, chemical, and thermal stability, and vast adsorption power along with good transmittance and exceptional specific surface area. These properties make it an outstanding medium for eliminating diverse contaminants (6–8). Also, various methods, namely temperature, microemulsion, and co-precipitation, have been utilized to prepare magnetic NPs (MNPs) (9,10). Regarding molecular recognition and specificity, aptamer-based sensing has clear advantages over established detection methods. However, the ability to synthesize MNPs with a narrow size distribution, specific shape, and surface architecture remains a key limitation of the current technology (11, 12).

The exciting field of nanotechnology involves the deliberate fabrication of NPs and the precise control and improvement of their characteristics to enable their numerous applications for scientific development (13–16). The most considerable characteristic is their ability to demonstrate amplified biological bioavailability because of transformations of the most essential parameters, namely size, morphology, and surface area (17). In general, nanoparticle manufacturing heavily utilizes both physical and chemical processes. While the physical approach may reach its boundaries regarding cost-effectiveness, the chemical synthesis requires the direct use of hazardous chemicals that could pose a risk to human health and the environment (18–22).The MnO_2 NPs garner considerable attention in research endeavors owing to their broad applicability across multiple domains, facilitated by the capability to manipulate their chemical properties through tailored modifications (23). The advantages of MnO_2 NPs stem from their unique properties and versatile applications across various fields. Some key benefits include gas sensing applications (24), biomedical applications, antibacterial properties, catalysis (25), optoelectronic devices, energy storage, photocatalysis, high surface area, and tunable properties (26,27). This study aims to remove Terasil black dye from water, particularly in textile industries. The nanocomposite was created using a co-precipitation method, followed by physical bonding with MnO_2 NPs.

2. Materials and Methods

2.1. Materials

Reduced graphene oxide (rGO), HCl with a concentration of 37%, $FeCl_3$, $FeSO_4.7H_2O$, NaOH, MnO_2 NPs, and deionized water were the sources of the chemicals. Merck and Sigma-Aldrich Co. (USA) were the source of all substances.

2.2. Synthesis of rGO/Fe_3O_4/MnO_2

Reduced graphene oxide was synthesized using the modified Hummers' method (2). In this experimental design, rGO was added as an ingredient of a 200 mL solution containing 0.6 M HCl with a concentration of 37%. This, in addition, was left to agitate for 45 minutes. Afterward, the remaining solution was treated with 28.4 g of $FeCl_3$, and the mixture was vigorously stirred for one hour. The admixture was then grown in the dark for the following hours. At the start of the overnight period, 18.8 g of $FeSO_4.7H_2O$ were put in the earlier solution, and the mixture was continuously stirred for 60 minutes. After that, 300 mL of 1M sodium hydroxide (NaOH) solution was dropped into the mixture with vigorous stirring at a temperature of 90°C until the pH reached 11, and it formed black precipitates of the rGO/Fe_3O_4 sheets. Filtration followed an intensive washing process of the precipitate obtained with deionized water and ethanol. The precipitates were then kept in a drying oven at 90°C with a drying period of five hours (28). The next step was the preparation of 1.25 g of the rGO/Fe_3O_4 material by dissolving this amount in 125 mL of DI water using sonication to enable diffusion. Afterwards, 1.75 g of MnO_2 was precisely weighed and added to the solution that contained the rGO/Fe_3O_4 composite. The liquid was rigorously shaken for 1 hour to ensure complete uniformization of the chemicals. The filtration procedure was done on the solution after the stirring process to separate the solid parts of the solution. The filtrate supplied was then dried at 80°C for a maximum of 5 hours to remove any remaining moisture in the obtained filtrate.

3. Results and Discussion

3.1. Characterization of rGO/Fe_3O_4/MnO_2 nanocomposite

The synthesized samples underwent characterization via X-ray diffraction (XRD), field emission scanning electron microscopy (FESEM), and energy dispersive X-ray (EDX) XRD, FESEM, and EDX techniques. The XRD analysis was employed to investigate the structural properties of rGO/Fe_3O_4/MnO_2 nano powder, while FESEM was utilized to examine surface morphology and nanoparticle size. Additionally, EDX was employed to assess the composition of the samples' elements. The XRD analysis of rGO/Fe_3O_4/MnO_2 nano powder indicates the formation of an amorphous phase. Notably, distinct diffraction peaks were observed at specific 2θ angles, as shown in **Table (1)** and **Figure (1).**

Table 1. The XRD analysis values of rGO/Fe_3O_4/MnO_2 nanocomposite

Pos. (°2Th.)	Height (cts)	FWHM Left (°2Th.)	d-spacing (Å)	Rel. Int. (%)	Tip Width
23.3110	192.09	0.4920	3.81602	13.13	0.5904
26.6568	710.56	0.2952	3.34416	48.57	0.3542
28.7959	128.01	0.7872	3.10043	8.75	0.9446
33.2046	1462.83	0.3444	2.69816	100.00	0.4133
38.4489	290.16	0.3936	2.34135	19.84	0.4723
42.9526	76.83	0.7872	2.10572	5.25	0.9446
45.3653	164.76	0.5904	1.99918	11.26	0.7085
49.5927	329.86	0.4920	1.83822	22.55	0.5904
55.4561	591.72	0.3444	1.65695	40.45	0.4133
64.3472	119.38	0.3936	1.44781	8.16	0.4723
66.0618	310.29	0.3936	1.41433	21.21	0.4723

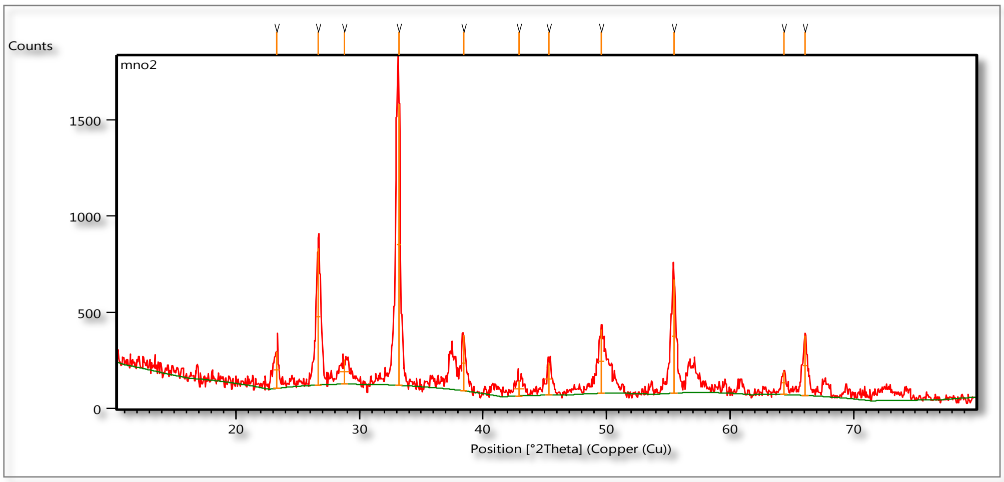

Figure 1. The XRD spectra of rGO/Fe_3O_4/MnO_2 nanocomposite

During morphological analysis conducted via FESEM, the average value of the dimension of particles equal to 83 nm, it was observed that the surface morphology of the sample revealed particles exhibiting predominantly irregular shapes and significant agglomeration, as depicted in **Figure (2).**

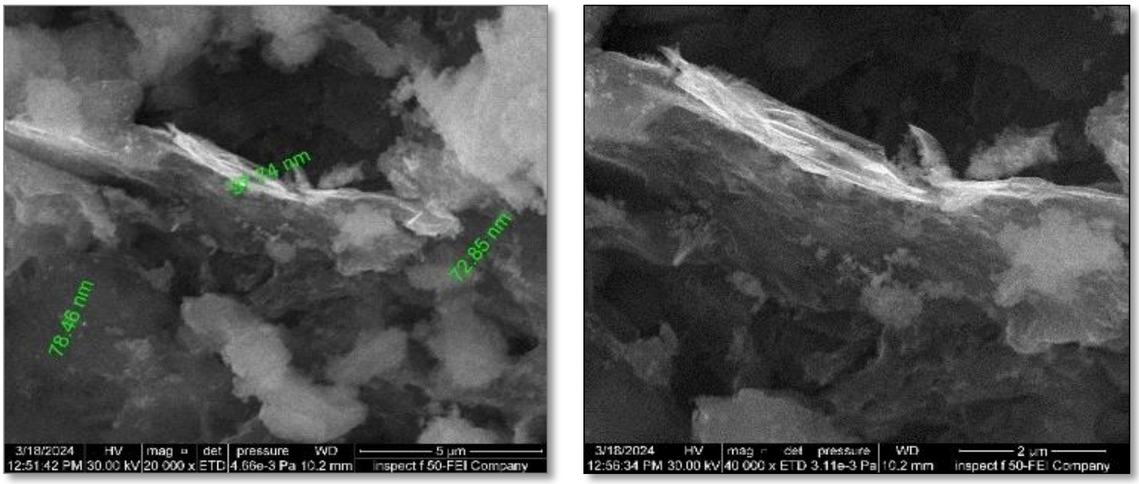

Figure 2. The FESEM images of rGO/Fe_3O_4/MnO_2 nanocomposite

The EDX characterization was conducted to determine the elemental composition of the rGO/Fe_3O_4/MnO_2 nanocomposite. The obtained spectra exhibited prominent peaks corresponding to elements, as illustrated in **Table (2)** and **Figure (3).**

Table 2. The EDX elemental composition of rGO/Fe_3O_4/MnO_2 nanocomposite

Element	Line Type	Apparent Concentration	k Ratio	Wt%	Wt% Sigma	Atomic %	Standard Label	Factory Standard
C	K series	2.24	0.02245	53.53	0.31	72.43	C Vit	Yes
O	K series	1.67	0.00560	19.30	0.24	19.61	SiO_2	Yes
Mn	K series	1.15	0.01150	12.14	0.21	3.59	Mn	Yes
Fe	K series	1.45	0.01446	15.02	0.25	4.37	Fe	Yes
Total:				100.00		100.00		

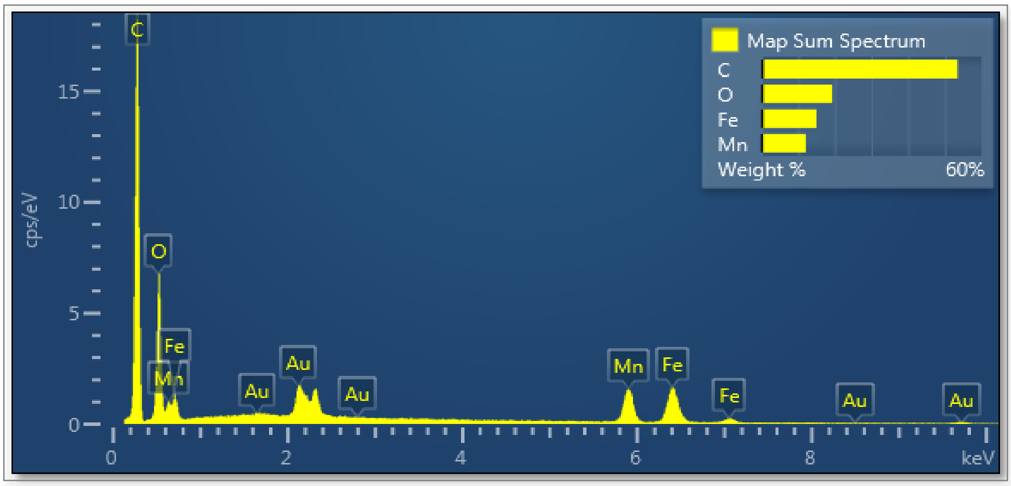

Figure 3. The EDX elemental composition of rGO/Fe_3O_4/MnO_2 nanocomposite

3.2. Calibration curve

This study prepared a series of standard solutions with known concentrations of Terasil Black dye solutions (10, 20, 40, 60, 80, 100, 120 ppm). By plotting absorbance (A) against concentration (C), a calibration curve is shown in **Figure (4)**, and it has been used to calculate concentration (C_t) at time (t) from the values of the absorbances of Terasil Black dye solution at a wavelength of $\lambda_{max.}$= 594 nm, the concentrations of the dye solution were obtained using the Beer-Lambert law:

$$A = \varepsilon\ c\ l \qquad (1)$$

A = Absorbance (unitless).

ε = Molar absorptivity (L mol^{-1} cm^{-1}), a constant specific to the substance.

c = Concentration of the solute (mol/L).

l = Path length of the cuvette (cm).

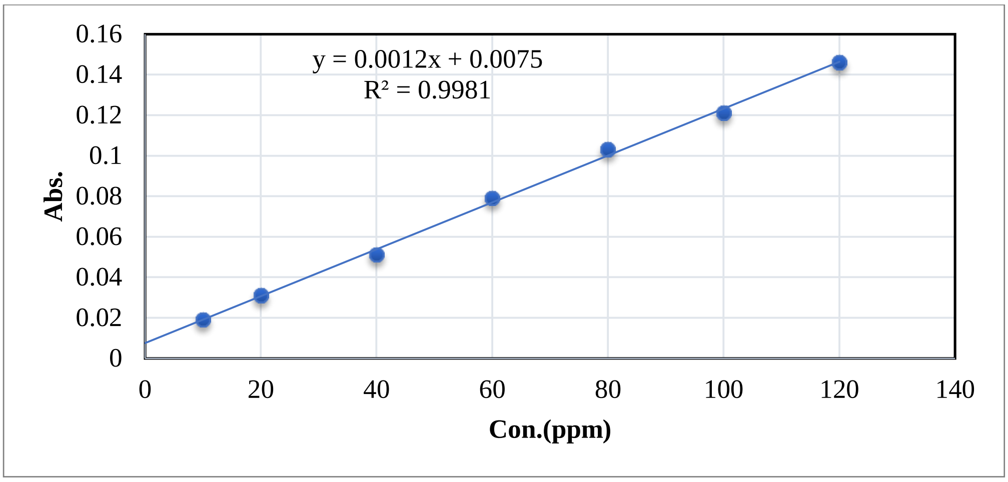

Figure 4. Calibration curve of Terasil Black at different concentrations

3.3. Contact time

The study investigated the time required for the adsorption process to attain equilibrium. That was done by utilizing a 100 ppm of Terasil Black dye, a temperature of 293K, a pH of 7, and an adsorbent dose of 0.025 g. Various contact periods were examined. **Figure (5)** illustrates the graph of (q_t) plotted against time (t), and by using the equation:

$$q_t = (C_o - C_t) \qquad (2)$$

Where the values of q_t, C_o, C_t, V, and m represent the amount of the adsorbate (mg/g) at time (t), the initial aqueous concentration (ppm), the concentration (ppm) at time (t), the solution volume (L), and the adsorbent weight (m), respectively. The contact periods indicate that the adsorption capacity of the dye increases as the contact time increases. Initially, the adsorption process occurred rapidly due to the abundance of binding sites present on the surfaces of the adsorbents. However, most of these sites would become occupied over time, reducing adsorption effectiveness. Depending on the scarcity of available active sites on the surface of the adsorbent, only a minimal quantity of dye may adhere. Once all the binding sites for the dye ions have been exhausted, the adsorbents reach a state of saturation and maintain a constant adsorption capacity. The equilibrium time of Terasil Black dye solution on $rGO/Fe_3O_4/MnO_2$ nanocomposite surface is 60 minutes, as shown in **Figure (5)**.

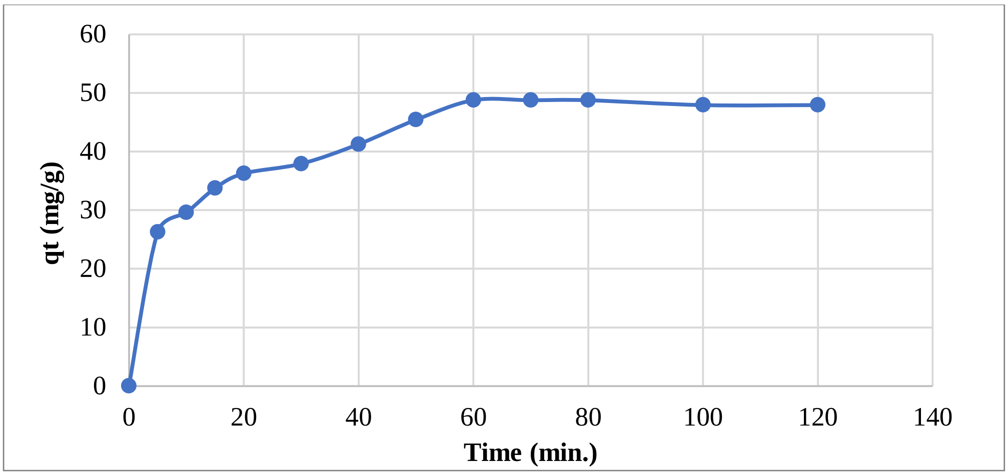

Figure 5. The contact time of Terasil Black on rGO/Fe_3O_4/MnO_2 nanocomposite surface at 293 K

3.4. Effect of change in temperature

The adsorption of Terasil Black dye from an aqueous solution was studied on the surfaces of rGO/Fe_3O_4/MnO_2 nanocomposites. A 250 mL of dye solution with varying concentrations was used, keeping other parameters such as pH= 7 and adsorbent dose (0.025 g) constant. The flask containing the solutions was placed in a shaker controlled by a thermostat, set at a speed of 100 cycles per minute. This was done for an equilibrium period of around 60 minutes, at temperatures of 288, 298, 308, and 318 Kelvin, specifically for the surface of the rGO/Fe_3O_4/MnO_2 nanocomposite.

The adsorption quantities (q_e, C_e) were recorded in **Table (3)** and **Figure (6)**. These values were determined using the equation:

$$q_e = (C_o - C_e)\, V/m \quad (3)$$

The values of q_e, C_o, C_e, V, and m represent the amount of the adsorbate, the initial aqueous concentration, the equilibrium concentration, the solution volume, and the adsorbent weight, respectively.

Adsorption isotherms provide essential knowledge about the adsorption process, including its circumstances, the adsorbed material's adsorption capability, and the concentration at which it occurs. It has been observed that the adsorption isotherm of Terasil Black dye on the surface of rGO/Fe_3O_4/MnO_2 nanocomposite follows the (S1) type according to the (Giles) classification, as in **Figure (6)**. The S-type isotherm is derived from Freundlich's fundamental adsorption principles. Heterogeneous surfaces result in this form of isotherm, where adsorption occurs with varying forces over various surface regions. The adsorption energy decreases as the surface coverage increases, as may be deduced during class (S), it was discussed that the orientation of adsorbed molecules on a surface might be perpendicular, meaning they were connected from one end. This vertical orientation allows the molecules to occupy less surface area, resulting in a higher adsorption rate.

Giles showed that the S class of isotherms represents non-chemical adsorption, indicating the existence of dispersion forces or hydrogen bonding. The activation energy provides insight into the likelihood of interactions. If the interaction forces between the adsorbent and the adsorbate were significant, the activation energy will be elevated, resulting in adsorption following the class (S) or the Freundlich isotherm. This implies that the adsorbent molecules arrange themselves in rows or clusters on the surface. This is supported by the isotherm shape, in which adsorption rises proportionally with the increase in equilibrium concentration.

Table 3. The quantity of the adsorbate and the equilibrium concentration of Terasil Black on $rGO/Fe_3O_4/MnO_2$ nanocomposite surface at four different temperatures

	288 Kelvin		298 Kelvin		308 Kelvin		318 Kelvin	
C_o	C_e(mg/L)	q_e(mg/g)	C_e(mg/L)	q_e(mg/g)	C_e(mg/L)	q_e(mg/g)	C_e(mg/L)	q_e(mg/g)
50	32.08333	17.91667	31.25	18.75	30.41667	19.58333	19.58333	30.41667
100	55.41667	44.58333	49.58333	50.41667	42.08333	57.91667	37.91667	62.08333
150	62.08333	87.91667	57.08333	92.91667	54.58333	95.41667	44.58333	105.4167
200	67.08333	132.9167	56.25	143.75	52.08333	147.9167	42.91667	157.0833
250	81.25	168.75	65.41667	184.5833	62.91667	187.0833	57.08333	192.9167
300	95.41667	204.5833	82.08333	217.9167	77.08333	222.9167	71.25	228.75

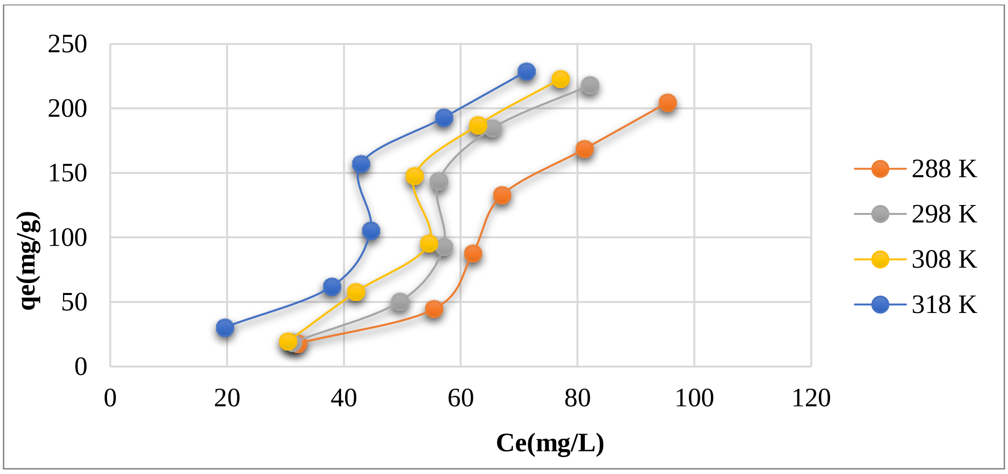

Figure 6. The adsorption isotherms of Terasil Black on $rGO/Fe_3O_4/MnO_2$ nanocomposite surface at four different temperatures

It has been observed that the amount of adsorbed material from the Terasil Black dye on the surface of the $rGO/Fe_3O_4/MnO_2$ nanocomposite increased when the dye concentration was increased. As the concentration increased, more dye molecules with positive charges showed up. This increased the electrostatic attraction between the dye molecules and the active sites on the surface, improving adsorption. On the other hand, as the temperature rises, we observe an increase in the quantity of material adsorbed. Higher temperatures provide the required activation energy for the dye ions to surpass the energy barrier needed for adsorption. This signifies the endothermic characteristic of the adsorption process and the presence of an absorption process alongside the adsorption process. As the temperature rises, the rate at which the dye molecules spread on both the surface and within increases. The adsorbent surface's holes facilitate the adsorption of Terasil Black dye on all surfaces, particularly at elevated temperatures.

3.5. Adsorption isotherms

The study focused on examining the adsorption isotherms of Terasil Black dye on the surfaces of $rGO/Fe_3O_4/MnO_2$ nanocomposites, which were used as adsorbents. Several models, such as the Freundlich, Langmuir, and Temkin models, may be used to explain the experimental data.

3.5.1. Freundlich model

The Freundlich isotherm is used to investigate the process of multilayer adsorption. This isotherm is derived from the process of adsorption in heterogeneous systems, and it is represented in the following manner (29):

$$q_e = K_F\, C_e^{1/n} \qquad (4)$$

Where q_e is the adsorption capacity (mg/g) and K_F is the Freundlich constant (L/g). **Figure (7)** depicts the linear Freundlich equation graphically, where $\ln q_e$ is plotted against $\ln C_e$, resulting in a straight line. The intercept of the line is $\ln K_F$, while the slope represents (1/n). K_F (L/g) denotes the adsorbed capacity, whereas n represents the adsorption intensity.

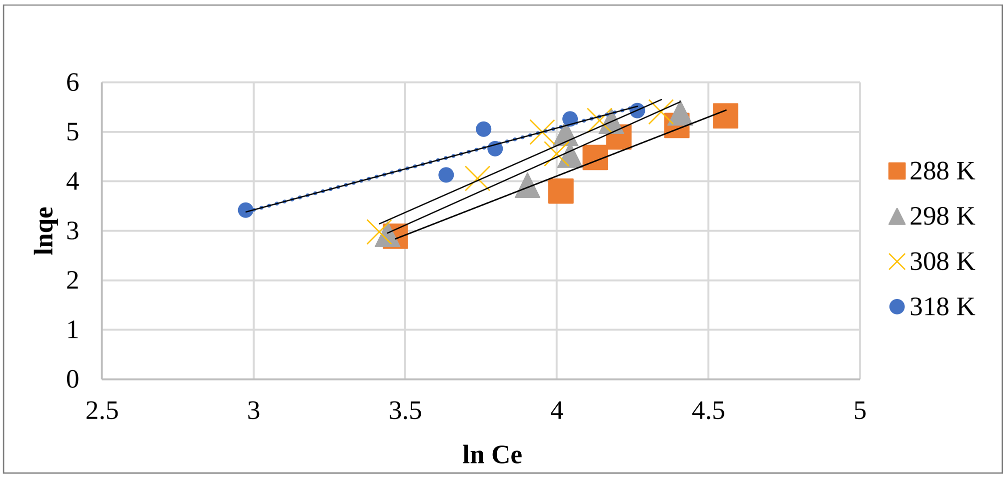

Figure 7. Linear Freundlich adsorption isotherm of Terasil Black on $rGO/Fe_3O_4/MnO_2$ nanocomposite surface at four different temperatures

Considering the data shown in **Table (4)**, it is evident that the variable (n) consistently increases. This parameter quantifies the adhesive strength between the surface of the $rGO/Fe_3O_4/MnO_2$ nanocomposite and other substances at various temperatures.

Table 4. Freundlich constants and correlation coefficient for the adsorption of Terasil Black on $rGO/Fe_3O_4/MnO_2$ nanocomposite surface at four different temperatures

	288 Kelvin	298 Kelvin	308 Kelvin	318 Kelvin
K_F	0.004374	0.001483	0.002268	0.213227
n	0.419252	0.363557	0.370041	0.603828
R^2	0.9464	0.9616	0.9285	0.9017

The observed rise indicates that the Terasil black dye is being physically adsorbed onto the surface of the nanocomposite. The K_F value of Terasil Black dye adhering to the surface of the $rGO/Fe_3O_4/MnO_2$ nanocomposite increases as the temperature increases, indicating that the adhesion mechanism is endothermic. Based on the correlation coefficient values (R^2) for the Freundlich model, it has been concluded that the Freundlich equation applies to the surface being studied. Nevertheless, its efficacy diminishes with rising temperatures. This indicates that adsorption processes occur on surfaces with diverse properties, resulting in many sites with variable levels of adsorption energy.

3.5.2. Langmuir isotherm model

The isotherm described specifically applies to adsorbent molecules that selectively bind to unoccupied sites on the surfaces of the adsorbent substances. Each site can accommodate just one atomic or molecular adsorbent species (30). The equation can be written as follows:

$$\frac{C_e}{q_e} = \frac{1}{q_{max}} * C_e + \frac{1}{q_{max}\, K_L} \tag{5}$$

The q_{max} value represents the highest adsorption capacity in (mg/g). In contrast, K_L refers to the Langmuir constant, which is associated with the affinity binding sites and energy of adsorption, (L/mg). The graphical representation of linear Langmuir equation in **Figure (8)** shows a plot of C_e/q_e vs C_e obtains in a straight line has an intercept equal to ($1/K_L\ q_{max}$) and a value of a slope is ($1/q_{max}$).

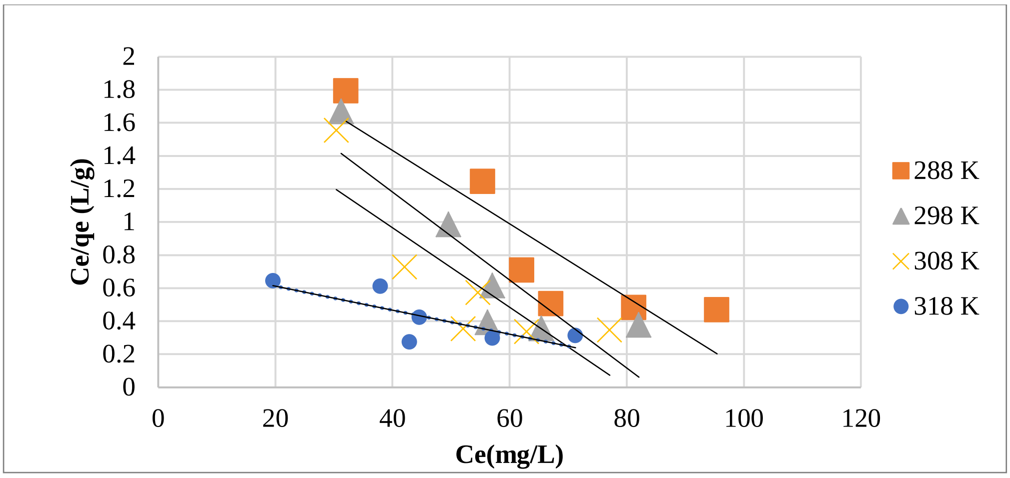

Figure 8. Linear Langmuir adsorption isotherm of Terasil Black on rGO/Fe_3O_4/MnO_2 nanocomposite surface at four different temperatures

The data in **Table (5)** shows the value of adsorbed Terasil Black on rGO/Fe_3O_4/MnO_2 nanocomposite surface at different temperatures. The above values show that the adsorption process obeys the Langmuir isotherm less than the Freundlich isotherm. The adsorption at maximum capacity (q_{max}) increased when the temperature increased, indicating that the adsorption density is enhanced at high temperatures. Moreover, the result shows that adsorption energy (K_L) increased when the temperature increased, which reveals a higher affinity between the above surface and Terasil Black dye.

Table 5. Langmuir constants and correlation coefficient for the adsorption of Terasil Black on rGO/Fe_3O_4/MnO_2 nanocomposite surface at four different temperatures

	288 Kelvin	298 Kelvin	308 Kelvin	318 Kelvin
q_{max}	-45.045	-37.594	-41.6667	-138.889
K_L	-0.00957	-0.01183	-0.01246	-0.00952
R^2	0.8015	0.7353	0.6845	0.5956

3.5.3 Temkin isotherm model

This model assumes a linear decrease in the synchronous temperature of the adsorption process for the molecules in the layer when the surface is covered due to interactions between the surface molecules and the adsorbent (31). The isotherm of Temkin is represented by the equation (6):

$$q_e = B \ln (A_T . C_e) \qquad (6)$$

Where B is the isotherm of Temkin constant, which is determined as follows: B = RT/b, R is the constant of the gas (8.314 J/K.mol), T is the temperature at the absolute state and b is the heat of adsorption (J/mol), A_T is the equilibrium binding constant representing the maximum binding energy (L/g).

The graphical representation of the linear Temkin equation in **Figure (9**) shows a plot of q_e vs ln C_e obtained in a straight line, with an intercept equal to (A_T) and a slope equal to (B_T).

From the results in **Figure (9)**, it was concluded that there was a good fit and reasonable accuracy; however, the calibration curve deviated slightly from the experimental data. The most suitable temperature was 308 Kelvin, as indicated by a coefficient of determination (R^2) of 0.8945.

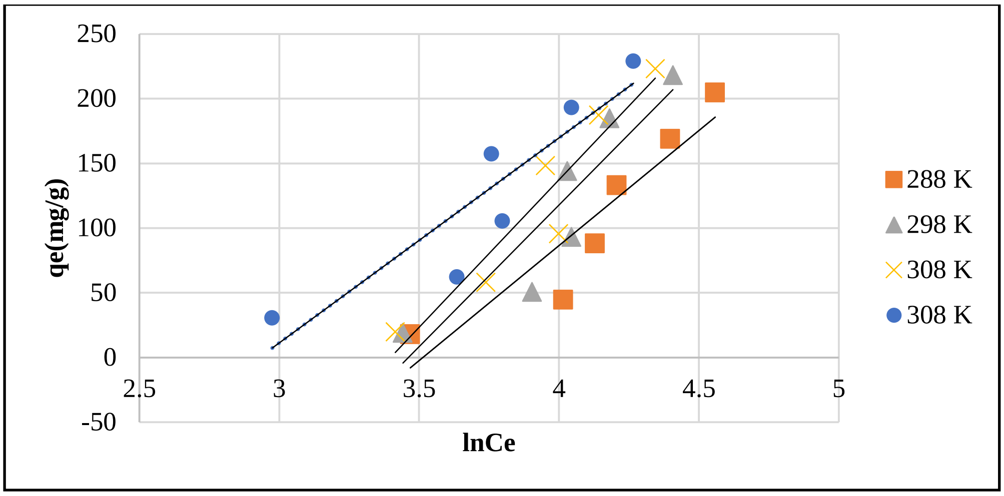

Figure 9. linear Temkin adsorption isotherm of Terasil Black on $rGO/Fe_3O_4/MnO_2$ nanocomposite surface at four different temperatures

Considering the data in **Table (6)**, it can be concluded that the low values of the heat of adsorption (BT) and the increase of Temkin isotherm constants (AT) with rising temperature indicate a preference for adsorption at high temperatures. This suggests that the system is suitable for physical adsorption and endothermic processes.

Table 6. Temkin constants and correlation coefficient for the adsorption Terasil Black on $rGO/Fe_3O_4/MnO_2$ nanocomposite surface at four different temperatures

	288 Kelvin	**298 Kelvin**	**308 Kelvin**	**318 Kelvin**
B_T	177.65	218.83	227.83	158.37
A_T	0.02981	0.031371	0.033453	0.053456
R^2	0.8585	0.8303	0.8945	0.8223

4. Conclusion

The adsorption isotherms of Terasil Black on the surface of $rGO/Fe_3O_4/MnO_2$ nanocomposite adsorbent exhibit an S-shaped pattern at various temperatures, as classified by Giles. This suggests that the dye ions were packed within clusters or rows on the adsorbent surface, aligned vertically, for the $rGO/Fe_3O_4/MnO_2$ nanocomposite. The adsorption of Terasil Black dye on the surfaces of $rGO/Fe_3O_4/MnO_2$ nanocomposites is primarily controlled by an endothermic and physical adsorption mechanism, which is intensified at elevated temperatures. The process exhibits a stronger adherence to the Freundlich isotherm, indicating that the adsorption process occurred on non-homogeneous surfaces. Both chemical and physical adsorption processes were involved at various temperature ranges.

Acknowledgment

The authors thank the Department of Chemistry at the College of Education for Pure Science (Ibn Al-Haitham) at the University of Baghdad, for providing chemicals and support.

Conflict of Interest

The authors declare that they have no conflicts of interest.

Funding

No funding.

Ethical Clearance

This work has been approved by the Scientific Committee at the Department of

Chemistry, College of Education for Pure Science (Ibn Al-Haitham), University of Baghdad.

References

1. Sadiq YM, Al-Abodi EE. Preparation and characterization of a new nano mixture, and its application as photocatalysis in self-assembly method for water treatment. In: AIP Conference Proceedings. 2019; 2190:020042. https://doi.org/10.1063/1.5138528 .
2. Hummers WS, Offeman RE. Preparation of graphitic oxide. J Am Chem Soc. 1958; 80(6):1339. https://pubs.acs.org/doi/pdf/10.1021/ja01539a017 .
3. Ahmed MA, Ahmed MA, Mohamed AA. Facile adsorptive removal of dyes and heavy metals from wastewaters using magnetic nanocomposite of zinc ferrite@reduced graphene oxide. Inorg Chem Commun. 2022; 144(3): 109912. https://doi.org/10.1016/j.inoche.2022.109912.
4. Huang Y, Ding X, Li S, Zhang N, Wang J. Magnetic reduced graphene oxide nanocomposite as an effective electromagnetic wave absorber and its absorbing mechanism. Ceram Int. 2016; 42(15): 17116-17122. https://doi.org/10.1016/j.ceramint.2016.07.223.
5. Sulaiman AF, Farouk A, Salman SA, Al-Dhahir TA, Al-Saadi TM, Al-Abodi EE. PEG-coated magnetite nanoparticles as adsorbents surface for remove methylene blue dye from aqueous solutions. In: AIP Conference Proceedings. 2019; 2190(1):20040. https://doi.org/10.1016/j.ceramint.2016.07.223.
6. Zamani A, Sadjadi MS, Mahjoub A, Yousefi M, Farhadyar N. Synthesis, characterization and investigation of photocatalytic activity of $ZnFe_2O_4$@MnO–GO and $ZnFe_2O_4$@MnO–rGO nanocomposites for degradation of dye Congo red from wastewater under visible light irradiation. Res Chem Intermediates. 2020; 46(8):33-61. https://doi.org/10.1007/s11164-019-03934-w.
7. El-Hout SI, El-Sheikh SM, Gaber A, Shawky A, Ahmed AI. Highly efficient sunlight-driven photocatalytic degradation of malachite green dye over reduced graphene oxide-supported CuS nanoparticles. J Alloys Compd. 2020; 849: 156573. https://doi.org/10.1016/j.jallcom.2020.156573.
8. Al-Abodi EE, Hashim A. Photo degradation of Congo red dye by using new nanocomposite. Annals of RSCB. 2021; 25(3):6822-6835. http://annalsofrscb.ro.
9. Musab L, Al-Abodi EE. Preparation and characterization composites contain of magnetic iron oxide nanoparticles with different weight ratios of dextrin, and using it to removal of heavy metals from aqueous solutions. In: Energy Procedia. 2019; 157:752-762. https://doi.org/10.1016/j.egypro.2018.11.241.
10. Kadhim RM, Al-Abodi EE, Al-Alawy AF. Citrate-coated magnetite nanoparticles as osmotic agent in a forward osmosis process. Desalin Water Treat. 2018; 115:45-52. https://doi.org/10.5004/dwt.2018.22456.
11. Al-Alawy AF, Al-Abodi EE, Kadhim RM. Synthesis and characterization of magnetic iron oxide nanoparticles by co-precipitation method at different conditions. J Eng. 2018; 24(10):60-72. https://www.iraqoaj.net/iasj/download/ff9e1bf295be4629
12. Jawad A, Al-Abodi EE. Investigating (Fe_3O_4) magnetic nanoparticles impregnated onto tri-sodium citrate to remove, of methylene blue dye from aqueous solutions. In: AIP Conference Proceedings. 2019; 2123:020026. https://doi.org/10.1063/1.5116953 .
13. Mahdia BO, Majeed ZH, Hussein SS, Abbas ZH, Hamood HH. Application of Nanotechnology in Geotechnical Engineering: A review. Saudi J Eng Technol. 2021; 6(6):143-151. https://doi.org/10.36348/sjet.2021.v06i06.005.
14. Hadi K, M. Al- Saadi T. Investigating the structural and magnetic properties of nickel oxide nanoparticles prepared by precipitation method. IHJPAS. 2022; 35(4):94-103. https://doi.org/10.30526/35.4.2872.
15. Husain A, Entisar E. Al-Abodi. A Review Article: Green synthesis by using different plants to preparation oxide nanoparticles. IHJPAS. 2023; 36(1):246–259. https://doi.org/10.30526/36.1.2933 .

16. Husain WM, Araak JK, Ibrahim OMS. Green synthesis of zinc oxide nanoparticles from (punica granatum l) pomegranate aqueous peel extract. Iraqi J. Vet. Med. 2019; 43(2):6-14. https://doi.org/10.30539/iraqijvm.v43i2.524 .
17. Maťátková O, Michailidu J, Miškovská A, Kolouchová I, Masák J, Čejková A. Antimicrobial properties and applications of metal nanoparticles biosynthesized by green methods. Biotechnol. Adv. 2022; 58:107905. https://doi.org/10.1016/j.biotechadv.2022.107905.
18. Thakur P, Thakur A. Introduction to nanotechnology. In: Synthesis and applications of nanoparticles. Springer, 2022. https://doi.org/10.1007/978-981-16-6819-7.
19. Bayda S, Adeel M, Tuccinardi T, Cordani M, Rizzolio F. The history of nanoscience and nanotechnology: From chemical-physical applications to nanomedicine. Molecules. 2020; 25(1):112. https://doi.org/10.3390/molecules25010112.
20. Omanović-Mikličanin E, Badnjević A, Kazlagić A, Hajlovac M. Nanocomposites: A brief review. Health Technol (Berl). 2020; 10(14):51-59. http://dx.doi.org/10.1007/s12553-019-00380-x.
21. Saïah FBD, Bettahar N. Comparative study on adsorptive efficiency assessment of Congo red dye from aqueous solutions using nanoporous zirconia oxides and anionic clays nanosheet. Desalin Water Treat. 2022; 254:260-273. https://10.5004/dwt.2022.28329.
22. Sonal S, Mishra BK. A comprehensive review on the synthesis and performance of different zirconium-based adsorbents for the removal of various water contaminants. CEJ. 2021; 424:130509. https://doi.org/10.1016/j.cej.2021.130509.
23. Li Y, Zhu X, Dong Y, Yang Y, Shen D, Li Z, Dang X, Qin Z, Fan K. Nanomedicine-enabled mild photothermal therapy strategies for enhanced antitumor treatment. Advanced Nano Biomed Research. 2024; 4(2300094):1-25. https://doi.org/10.1002/anbr.202300094 .
24. Nunes D, Pimentel A, Goncalves A, Pereira S, Branquinho R, Barquinha P, Fortunato E, Martin R. Metal oxide nanostructures for sensor applications. Semicond Sci Technol. 2019; 34(4):043001. https://doi.org/10.1088/1361-6641/ab011e.
25. Waghmode MS, Gunjal AB, Mulla JA, Patil NN, Nawani NN. Studies on the titanium dioxide nanoparticles: biosynthesis, applications and remediation. SN Appl Sci. 2019; 1(4):1-9. https://doi.org/10.1007/s42452-019-0337-3 .
26. Alabodi EE, Abdlzhra AF, Abdllatief IA. Preparation and characterization of silver nanoparticles and study their effect on the electrical conductivity of the polymer blend(poly vinyl acetate. pectin, poly aniline). IHJPAS. 2016; 29(3):379–389.
27. Saeed ZA, Aadim KA. Study of optical, structural and morphology properties of tin oxide nanoparticles by pulse laser ablation and its effect on bacteria Staphylococcus aureus. IJS. 2023; 64(11):5654–5664 https://doi.org/10.24996/ijs.2023.64.11.17.
28. Aisida SO, Akpa PA, Ahmad I, Zhao T kai, Maaza M, Ezema FI. Bio-inspired encapsulation and functionalization of iron oxide nanoparticles for biomedical applications. Eur Polym J 2020; 122: 109371. https://doi.org/10.1016/j.eurpolymj.2019.109371.
29. Freundlich H, Kroepelin H. Über die Kinetik der Umwandlung von Halogenalkylaminen in heterocyclische Verbindungen. IV. Zeitschrift für Physikalische Chemie. 1926;122U(1):39-48. https://doi.org/10.1515/zpch-1926-12204
30. Langmuir I. The adsorption of gases on plane surfaces of glass, mica and platinum. J Am Chem Soc. 1918; 40(9):1361-1403. https://doi.org/10.1021/ja02242a004.
31. Tempkin MJ, Pyzhev V. Recent modification to Langmuir isotherms. Acta Physiochem USSR. 1940; 12:217-225. https://www.sid.ir/paper/608793/en .